PCCP

Accepted Manuscript

ROYAL SOCIETY OF CHEMISTRY

www.rsc.org/pccp

Magnetocaloric effect with critical behavior of a periodic Anderson-like organic polymer

L. J. Ding*, Y. Zhong, S. W. Fan, and L. Y. Zhu

Department of Physics, China Three Gorges University, YiChang 443002, China

*To whom correspondence should be addressed. E-mail: dinglinjie82@126.com (L. J. Ding)

We study the magnetocaloric effect and critical behavior of a periodic Anderson-like organic polymer using Green's function theory, in which the localized f orbitals hybridize with the conduction orbitals at even sites. The field-induced metal-insulator transitions with the magnetic Grüneisen parameter showing $|\Gamma_h| \sim T^{-1}$ power-law critical behaviour are revealed, which provides a new thermodynamic means for probing quantum phase transitions. It is found that the competition of up-spin and down-spin hole excitations is responsible for the double peak structure of magnetic entropy change ($-\Delta S$) for the dominant Kondo coupling case, implying a double magnetic cooling process via demagnetization, which follows a power law dependence of magnetic field h: $-\Delta S \sim h^n$. The local exponent n tends to 1 and 2 below and above T_C, while has a minimum 0.648 at T_C, which is in accordance with the experimental observation on perovskite manganites $Pr_{0.55}Sr_{0.45}MnO_3$ and $Nd_{0.55}Sr_{0.45}MnO_3$ (J. Y. Fan et al., Appl. Phys. Lett., 2011, **98**, 072508; Europhys. Lett., 2015, **112**, 17005) corresponding to the conventional ferromagnets within the mean field theory $-\Delta S \sim h^{2/3}$. At T_C, the $-\Delta S \sim h$ curves with convex curvature superpose each other for small V values, which are separated by the large V case, distinguishing the RKKY interaction and Kondo coupling explicitly. Furthermore, the critical scaling law $n(T_C)=1+(\beta-1)/(\beta+\gamma)=1+1/\delta(1-1/\beta)$ is related to the critical exponents (β, γ, and δ) extracted from the Arrott-Noakes equation of state and Kouvel-Fisher method, which fulfill the Widom scaling relation $\delta=1+\gamma\beta^{-1}$, indicating self-consistency and reliability of the obtained results. In addition,

based on the scaling hypothesis through checking the scaling analysis of magnetization, the *M*-*T*-*h* curves collapse onto two independent universal branches below and above T_C.

1. Introduction

Recently magnetocaloric effect (MCE) has been intensively studied in a great number of magnetic materials due to their potential application in magnetic refrigeration,[1-11] which was proposed as an environmentally friendly and energy-efficient cooling technique. In a magnetic cooling cycle, the magnetic material is a crucial part of system design, because heat is pumped in and out through the material and cooling performance is dependent on its ability to generate and reverse heat. One important issue related to magnetic refrigeration is to understanding how the MCE evolves with the magnetic field and temperature, which is helpful for the deeper understanding of magnetic phase transitions.[12,13] Usually, the MCE was used as a powerful tool for investigation of magnetic phase transitions accompanying spin structure transformations. Especially, a class of magnetic materials is governed by pronounced quantum many-body effects, in which the MCE has been used to study the quantum criticality arising from quantum fluctuations. A map of the entropy landscape can identify various quantum phases.[14] Moreover, the magnetic Grüneisen parameter Γ_h, related to the cooling rate, displays sign change close to the quantum critical point (QCP) signaling an accumulation of entropy, which was regarded as an important tool to identify and classify a QCP by its divergence near a field-induced quantum phase transition (QPT), giving a very direct way to extract the critical exponents of QCP.[13,15] Meanwhile, the underlying QPT manifests itself at finite temperatures in an unusual sensitivity of thermodynamics under different fields. Additionally, the MCE is an intrinsic property for all magnetic materials wherein the entropy changes with magnetic field. Accordingly, the isothermal entropy change ($-\Delta S$) plays a

crucial role in the performance of magnetic cooling. In contrast to inorganic magnets, organic magnets are drawing attention in light of their lightness, flexibility and unbreakable.[6-11,16,17] To pursue large -Δ*S*, recently, many explorations focused on constructing various clusters or coordination polymers through selecting suitable metal ions and ligands. Some compounds were obtained such as $[\{Gd(OAc)_3(H_2O)_2\}_2]\bullet 4H_2O$, $Gd(OH)CO_3$, $[Na_2Mn_3(SO_4)_3(\mu_3\text{-}OH)_2(\mu_2\text{-}OH_2)_2]_n$ and so on.[8-10] It is worth noting that in the triangular $[Mn_3]$ cluster-based ferrimagnet,[10] the competition of the ferromagnetic and antiferromagnetic interactions plays a crucial role on enhancing MCE, which obeys the Lieb-Mattis theory.[18]

In addition, it has been shown that the field dependence of magnetocaloric parameters was associated with the intricate nature of magnetic phase transition and parametrized by critical exponents governing the transitions.[19-23] The analysis of the critical behavior can also provide significant information about the thermodynamic observations near the transition temperature T_C. For a continuous ferromagnetic transition, the critical behavior near T_C is characterized by a set of critical exponents β, γ, and δ.[19,20,22,23] The Arrott plot is the most straightforward approach in the form of M^2 versua h/M with parallel lines signaling the mean-field values β=0.5 and γ=1.0. To further refine the critical exponents, the isotherms are extrapolated to the M^2=0 and h/M=0 axes to obtain the spontaneous magnetization M_s(T) and $\chi_0(T)$, respectively, a power law fitting to which will yield the values of β and γ.[24] By using the critical exponents as a starting point, we can obtain a modified Arrott plot $M^{1/\beta}$ versus $(h/M)^{1/\gamma}$ with iteration procedures to restore parallel straight isotherm lines and get correct critical exponents, until β and γ converge.

Based on the Lieb-Mattis theory, Ovchinnikov[25] firstly proposed a synthesis of alternate hydrocarbon with high-spin ground state, as schematically illustrated in Fig. 1(a). The spin gap

and magnon excitations were investigated by employing Hubbard model.[26,27] Likewise, it was developed as a periodic Anderson-like model (PALM).[28,29] The *f* electrons are strongly localized, while the conduction electrons form a conduction sea distribute throughout the main zigzag chain, which presents a Fermi liquid coupling with localized spins, wherein two interactions compete for dominance. One interaction is the Kondo coupling for the localized spins screened by the conduction sea; the other is the superexchange, i.e., the indirect Ruderman-Kittel-Kasuya-Yosida (RKKY) interaction between the neighboring localized spins mediated by the conduction sea.[30,31] For the symmetrical case, the Kondo coupling $J_K \sim V^2/U$ gives rise to the fact that the behavior of the system is controlled by two parameters: the hybridization V between the conduction and localized *f* orbitals, and the Hubbard repulsion U on the localized *f* orbital.[32] Thus, the competition between Kondo coupling and RKKY interaction is attributed to the consequence of interplay between Coulomb interaction and hybridization. For this PALM, the ground state, ferrimagnetic and metal-insulator phase transitions were studied in detail.[28,29] However, in a magnetic field, the competition between Kondo coupling and RKKY interaction responsible for enhancing MCE will shed light on the critical behavior for the strong correlation electron system. Simultaneously, a systematic study of scaling analysis of the temperature and field dependence of magnetization will be carried out. A double peak structure in magnetic entropy change manifests a double magnetic cooling process. Thus, it is quite necessary to take a deeper investigation on the MCE and critical behavior for this PALM. In the forthcoming section, the model Hamiltonian and many-body Green's function method are presented. In section 3, the field-induced phase diagram associated with quantum criticality is explored; the MCE and critical scaling behavior are also analyzed and discussed. Finally, we draw a conclusion in section 4.

2. Model and Method

The organic polymer illustrated in Fig. 1(a) is described as a quasi-one-dimensional PALM, wherein the conduction electrons with uncorrelated orbitals reside in the main zigzag chain form a conduction sea, while a correlated localized *f* orbital locates at the side radical *R*. In an external magnetic field, it is governed by the following Hamiltonian,

$$H = -t\sum_{l,\sigma}\left(c^{+}_{l,1,\sigma}c_{l,2,\sigma} + c^{+}_{l,2,\sigma}c_{l+1,1,\sigma} + h.c\right) + \sum_{l,\sigma}\varepsilon_f c^{+}_{l,f,\sigma}c_{l,f,\sigma} + U\sum_{l} n^{f}_{l,\uparrow}n^{f}_{l,\downarrow}$$

$$+V\sum_{l,\sigma}\left(c^{+}_{l,2,\sigma}c_{l,f,\sigma} + h.c\right) - \frac{h}{2}\sum_{l}\sum_{\eta=1,2,f}\left(n^{\eta}_{l,\uparrow} - n^{\eta}_{l,\downarrow}\right). \qquad (1)$$

Herein, t denotes the hopping integral between the nearest-neighboring conduction orbitals, $c^{+}_{l,\eta,\sigma}\left(c_{l,\eta,\sigma}\right), n^{\eta}_{l,\sigma} = c^{+}_{l,\eta,\sigma}c_{l,\eta,\sigma}\left(\eta = 1,2\right)$ are the creation (annihilation) and number operators with spin $\sigma = \uparrow,\downarrow$ for conduction electrons. Nevertheless, $c^{+}_{l,f,\sigma}\left(c_{l,f,\sigma}\right)$ denotes the creation (annihilation) operator of localized f electron in the side radical R with bare energy ε_f and Coulomb repulsion U. In addition, V is the hybridization strength of the localized f electron with the conduction orbital (l,2), and $h = g\mu_B B$ is the reduced magnetic field (Zeeman energy).

Now, the Green's function method[33] is employed to decouple the Hamiltonian (1), which is defined as

$$G^{\sigma}_{ij}\left(t_1 - t_2\right) = << c_{i,\sigma}\left(t_1\right); c^{+}_{j,\sigma}\left(t_2\right) >> = -i\theta\left(t_1 - t_2\right) < c_{i,\sigma}c^{+}_{j,\sigma} + c^{+}_{j,\sigma}c_{i,\sigma} >, \qquad (2)$$

where the subscripts i and j number the lattice sites. After the time Fourier transformation, it is put into the equation of motion,

$$\omega << c_{i,\sigma}; c^{+}_{j,\sigma} >> = < [c_{i,\sigma}, c^{+}_{j,\sigma}]_{+} > + << [c_{i,\sigma}, H]; c^{+}_{j,\sigma} >> . \qquad (3)$$

By performing the equation of motion analogous to Eq. (3) for the high-order Green's function $<< [c_{i,\sigma}, H]; c^{+}_{j,\sigma} >>$, a higher-order Green's function will appear on the right side, resulting in an infinite set of coupled equations. In terms of Wick's theorem, we adopt the decoupling scheme

for the four-operator Green's functions,[34]

$$<< A^{+}BC;D^{+} >>\approx< A^{+}B ><< C;D_{+} >> - < A^{+}C ><< B;D^{+} >> . \quad (4)$$

Meanwhile, it is important to introduce the Green's functions for each spin channel (up-spin and down-spin) respectively, i.e., the Green's functions are diagonal in spin space $G_{ij}^{\sigma\sigma'} = G_{ij}^{\sigma}\delta_{\sigma\sigma'}$. For further Fourier transformation into *k*-space, the Green's function can be expressed as

$$G_{ij}^{\sigma} = \frac{1}{N}\sum_{k} g^{\sigma}(k,\omega) e^{ik\cdot(i-j)} . \quad (5)$$

The integral of the wavevector *k* extends over the first Brillouin zone. So, the momentum space Green's function $g^{\sigma}(k,\omega)$ can be described as a function of wavevector *k* and the elementary excitation spectrum $\omega = \omega(k)$.

According to the standard spectral theorem, the correlation function of the product of the electron operators can be calculated through the corresponding Green's function $g^{\sigma}(k,\omega)$

$$\left\langle c_{j,\mu,\sigma}^{+} c_{i,\nu,\sigma} \right\rangle = \frac{i}{2\pi N}\sum_{k} e^{ik\cdot(i-j)} \int \frac{g_{\mu\nu}^{\sigma}\left(k,\omega+i0^{+}\right) - g_{\mu\nu}^{\sigma}\left(k,\omega-i0^{+}\right)}{e^{\beta\omega}+1} d\omega , \quad (6)$$

where $\beta = 1/k_B T$, k_B is the Boltzman's constant, and *T* is the absolute temperature.

The spin density (sublattice magnetization) at one site is defined as

$$\left\langle S_{i,\eta}^{z} \right\rangle = \frac{1}{2}\left(\left\langle n_{i,\uparrow}^{\eta} \right\rangle - \left\langle n_{i,\downarrow}^{\eta} \right\rangle\right), (\eta = 1, 2, f) . \quad (7)$$

Then the average magnetization of the unit cell *M* and magnetic susceptibility χ are expressed as

$$M = \frac{1}{N}\sum_{i}\left(\left\langle S_{i,1}^{z} \right\rangle + \left\langle S_{i,2}^{z} \right\rangle + \left\langle S_{i,f}^{z} \right\rangle\right), \chi = \frac{\partial M}{\partial h} . \quad (8)$$

Likewise, the specific heat can be attained as

$$C_V = \frac{dE}{dT} = \frac{d\left\langle H \right\rangle}{dT} . \quad (9)$$

Accordingly, we can get the entropy,

$$S = \int_0^T \frac{C_V}{T'} dT' . \tag{10}$$

The magnetic entropy change is obtained as[1,2]

$$\Delta S = S(T,h) - S(T,0) = \int_0^T \frac{C_V(T',h) - C_V(T',0)}{T'} dT' = \int_0^h \left(\frac{\partial M}{\partial T}\right)_h dh . \tag{11}$$

Likewise, the magnetic Grüneisen parameter is expressed as[12,13]

$$\Gamma_h = \frac{1}{T}\left(\frac{\partial T}{\partial h}\right)_S = -\frac{(\partial S/\partial h)_T}{T(\partial S/\partial T)_h} = -\frac{1}{C_V}\left(\frac{\partial M}{\partial T}\right)_h . \tag{12}$$

Thereby, the above equations can be solved self-consistently. In calculation, an initial state, composed of a set of electron number and spin density of *f* orbital, is put into the equations to produce resultant values. The iteration goes on until convergence is reached.

3. Results and Discussion

In what follows, we set the hopping integral t=1.0, and all parameters are in units of it. We consider the symmetrical case $U + 2\varepsilon_f = 0$ without charge fluctuation. As an external magnetic field is turned on, it may undergo insulator-metal and magnetic phase transitions. Fig. 1(b) presents the field-induced ground state phase diagram, wherein the ferrimagnetic insulator, metal and ferromagnetic insulator phases are unveiled. As V ascends, the metallic region becomes narrower, which is ascribed to the enhancement of Kondo coupling. In order to identify the electric and magnetic states, the energy bands are plotted in Fig. 1(c)-(e). The Fermi level is located at E_F=0. At low field, Fig. 1(c) shows that two up-spin and one down-spin bands are occupied with an energy gap for large V, indicating the ground state lies in ferrimagnetic insulating state because of the dominant Kondo coupling. As V decreases, the insulating behavior becomes weaker and it undergoes a transition into metallic state, as shown in Fig. 1(d), wherein one up-spin and one down-spin bands transverse the Fermi level, as a result from the enhanced

RKKY interaction. However, as the field is very large, all the up-spin bands are pulled down into Fermi sea with an energy gap opened up (see Fig. 1(e)), resulting in the spin polarized ferromagnetic insulating state. Furthermore, the gapless and gapped low-lying excitations are also identified by the temperature dependence of entropy S, as shown in Fig. 1(f). One can find that the entropy asymptote presents activated behaviour because of the existence of finite energy gap between the ground and excited states for insulating phases, which is clearly manifested by the ln(S)-1/T curve at low temperature in the inset, wherein ln(S) behaves linearly with 1/T, giving rise to $S \propto e^{-\Delta/k_B T}$, the slope of which reflects the magnitude of energy gap ($-\Delta$). However, for the metallic phase, the entropy behaves T-linearly at ultra-low temperature, implying gapless ground state.

In order to present the competition between Kondo coupling and RKKY interaction responsible for the ferrimagnetic nature, the spin density (sublattice magnetization) for V=1.0 and 2.0 is performed and plotted in Fig. 2(a). One can find that for weak hybridization V, the localized f spin mainly contribute to the ferrimagnetism with relatively high transition temperature T_C, because the RKKY interaction is dominant. Nevertheless, as V ascends, the transition temperature T_C decreases with the ferrimagnetism mainly coming from the orbital (l,1). It is ascribed to the more and more dominant Kondo screening between orbitals (l,2) and (l,f). However, in a magnetic field, it presents a 1/3 magnetization plateau with two transition fields (see Fig. 2(b)), suggesting ferrimagnetic ground state and metal-insulator transitions. Furthermore, we anticipate that the QPTs will be reflected by the magnetocaloric properties at finite temperatures. From Fig. 2(c), one can clearly see that the quantum criticality can be identified explicitly for the entropy contour plots with sufficiently small value, and the QPTs are demonstrated by the dips of isoentropes. The

accumulation of entropy close to the transition fields indicates that the system is maximally undetermined which ground state to chose. Besides, the field dependence of Grüneisen ratio Γ_h proportional to the magnetic cooling rate for different temperatures is plotted in Fig. 2 (d), which presents the very sharp and pronounced positive peaks and negative valleys around the transition points at ultra-low temperature. Making contact with the argumentation of Garst,[13] the Grüneisen ratio Γ_h displays a characteristic divergent behaviour close to the transition point and changes sign as the field crosses it. However, with temperature ascending, all features become broader with the peaks reduced, and last will be washed out attributed to the strong thermal fluctuations driven the system to excited state without QPTs.

At different phases, the thermodynamics behave diversely, especially at the QCPs. Fig. 3(a) shows the magnetization against $T^{1/2}$ under different fields. One can find that the entrance into the gapless metal state is marked with a minimum or a maximum (see the arrow) in the magnetization, which provides a simple way to feature the phase boundary of gapless metal phase at finite temperature well. It is notable that the magnetization develops a $T^{1/2}$ behavior (linear relation of M-$T^{1/2}$ curve) as h approaches h_c. When h is close to h_s, we obtain a characteristic decrease $M\sim -T^{1/2}$. Besides, the temperature dependence of entropy at critical fields is presented in Fig. 3(b). It behaves $T^{1/2}$-linearly, different from that in the gapped and gapless phases. More generally, the results emphasize that the Grüneisen ratio Γ_h provides a novel thermodynamic means for probing QPTs. Fig. 3(c) shows that with decreasing temperature, Γ_h changes its sign in the gapless phase. Nevertheless, its absolute value increases gradually in gapped state for $h<h_c$ and $h>h_s$. It is worth noting that when h approaches h_c or h_s, Γ_h diverges rapidly upon cooling down to zero temperature, which provides a new way to explore QCPs. The double-logarithmic scale is plotted in Fig. 3(d) to

demonstrate the occurring $|\Gamma_h| \sim T^{-1}$ power-law critical behaviour, which has been observed on spin ladder system experimentally.[15]

At finite temperature, the system will manifest MCE under different magnetic fields. In Fig. 4(a)-(b), the magnetic entropy change against temperature are plotted for V=1.0 and 2.0, respectively. Recalling Fig. 1(d), as the field extends h_c but is nearby, the intermediate down-spin and up-spin energy bands cross the Fermi level slightly, making the excitations with minus energies become the hole type.[29] Thus, the magnetic entropy change $-\Delta S$ is closely related to the competition of the down-spin and up-spin hole excitations. For $h<h_c$, the magnetic field can open up the energy gap, and then close it. First, the energy gap is washed out by thermal fluctuations at low temperature, after that, the up-spin hole excitation crossover into down-spin one occurs, giving rise to only a sharp peak in $-\Delta S$ at T_C with broadened temperature region. Nevertheless, it is worth noting that the maximum of $-\Delta S$ is larger for larger V value due to the larger hole density of states resulting from the dispersion relation of energy bands, which indicates that strong Kondo coupling is benefit for low temperature cooling at low field. As h exceeds h_c, the up-spin band above E_F is pulled down into Fermi sea partially, while the down-spin one below E_F is pushed up partially. At this time, after the few up-spin holes are occupied, the down-spin ones will be excited, giving rise to a shoulder in $-\Delta S$ at high temperature. However, as the field gets across $(h_c+h_s)/2$, the $-\Delta S$ presents a double-peak structure for strong Kondo coupling (V=2.0) (see Fig. 4(b)), implying double magnetic refrigeration process at moderate field. In this case, the density of states of down-spin holes is larger than that of the up-spin ones near the Fermi level, yielding more down-spin holes excited at low temperature firstly, which contributes to the first peak of $-\Delta S$. After that, the up-spin holes will be excited responsible for the high temperature peak. While for

strong RKKY interaction (V=1.0) case, the strong dispersion relation of down-spin band (see Fig. 1(d)) yields less down-spin hole excitations at low temperature, thus resulting in that the first peak of $-\Delta S$ collapses into a shoulder (see Fig. 4(a)). For the field high enough ($h>h_s$), the low temperature peak vanishes gradually and the high temperature peak becomes higher with wider temperature region, because the energy gap becomes larger and only the up-spin holes will be excited.

Furthermore, it should be pointed out that $-\Delta S$ follows a power-law dependence of h: $-\Delta S \sim h^n$ (see the insets in Fig. 5(a) and (c)) with n the local exponent, which can be calculated via the relation: $n = \frac{d\ln(|\Delta S|)}{d\ln(h)}$.[21] Different from the antiferromagnets, wherein n is $\sim$2 for the entire temperature range at low fields,[21] one can find that the local exponent n is strongly dependent of temperature as shown in Fig. 5(a) and (c), demonstrated by the linear relation of $\ln(|\Delta S|)$ versus $\ln(h)$ with different slopes for different temperatures. At low temperatures well below T_C, n tends to 1 for a ferrimagnetic system, while tends to 2 at temperatures above T_C as a consequence of the Curie-Weiss law (see the insets in Fig. 5(b) and (d)). This scaling behavior is similar to that occurred in ferromagnetic materials.[19,35] In addition, n has a minimum at the transition temperature T_C, which is clearly illustrated in Fig. 5(b) and (d).

In order to explore the minimum of local exponent n and distinguish the domination of RKKY interaction and Kondo coupling, we plot the field dependence of $-\Delta S$ for different V values at T_C in Fig. 6(a). It is clearly seen that the $-\Delta S$-h curve presents a convex curvature, indicating n<1, which is unlike the case below or above T_C. Interestingly, for small V values, the curves superpose each other, separated with the large V case, which provides a new thermodynamic means to distinguish RKKY interaction and Kondo coupling in strong correlation electron system. Fig. 6(b) presents a

nearly parallel linear relation of $\ln(-\Delta S)$-$\ln(h)$ curve at T_C with n=0.648 for different V values, which is basically consistent with the experimental observation on perovskite manganites $Pr_{0.55}Sr_{0.45}MnO_3$ and $Nd_{0.55}Sr_{0.45}MnO_3$ corresponding to the conventional ferromagnets taking the mean field value 2/3.[22,23,36,37] The linear fits in Fig. 6(c) demonstrate the validity of the relationship $-\Delta S \propto h^{0.648}$ around T_C that characterize a second order phase transition, which is close to $-\Delta S \propto h^{2/3}$ for conventional ferromagnets obeying the mean field theory.[36,37]

Of particular interest is the scaling law related to the critical exponent β, γ, and δ, which obey the following relation at T=T_C:[19,20,22,23]

$$n(T_C) = 1 + (\beta - 1)/(\beta + \gamma) = 1 + 1/\delta(1 - 1/\beta). \quad (13)$$

Herein, the critical exponents (β, γ, and δ) are determined by a detailed scaling analysis based on the Arrott-Noakes equation of state,[38] which are defined for the spontaneous magnetization $M_s(T)$, inverse initial susceptibility χ_0^{-1}, and critical isotherm ($M(h)$) at T_C with the reduced temperature t=(T-T_C)/T_C as follows:[20,24,38-41]

$$M_s(T) \propto |t|^{\beta} \qquad T < T_C, \quad (14)$$

$$\chi_0^{-1}(T) \propto |t|^{\gamma} \qquad T > T_C, \quad (15)$$

$$M(h) \propto h^{1/\delta} \qquad T = T_C. \quad (16)$$

Thus, we can know that the critical behavior is determined by the critical exponents, but not by the critical temperature. For V=1.0, from the temperature dependence of M_s and χ_0^{-1}, we can get β=0.473 and γ=0.99 with T_C=0.283, as shown in Fig. 7(a) and (b), respectively. Accurately, the critical exponent β and γ can be determined by the Kouvel-Fisher (KF) method:[42]

$$\frac{M}{dM/dT} = \frac{T - T_C}{\beta}, \qquad \frac{\chi^{-1}}{d\chi^{-1}/dT} = \frac{T - T_C}{\gamma}. \quad (17)$$

Accordingly, the temperature dependence of $M/(dM/dT)$ and $\chi^{-1}/(d\chi^{-1}/dT)$ will yield straight lines

with slopes $1/\beta$ and $1/\gamma$, as plotted in the insets in Fig. 7(a) and (b) respectively. It gives us the critical exponents β=0.482 and γ=0.976 at T_C by KF method, which are close to those deduced from the Arrott-Noakes equation of state. Besides, according to Eq. (16), we plot the double-logarithm of h-M curve in Fig. 7(c), which shows a straight line with slope $1/\delta$ at T_C. Thus, we can obtain δ=3.041. According to the statistic theory, these critical exponents should fulfill the Widom scaling relation:[43]

$$\delta = 1 + \gamma/\beta . \qquad (18)$$

As a result, δ=3.093 and δ=3.025 are obtained from the Arrott-Noakes equation of state and KF method, which are close to that obtained from the critical isotherm analysis. It is demonstrated that these critical exponents are reliable and unambiguous for their self-consistency. Furthermore, from Eq. (13), we can get $n(T_C)$=0.64 and $n(T_C)$=0.645 from the Arrott-Noakes and KF methods, respectively, which approach the MCE measurement. For V=2.0, one can get (β, γ)=(0.479, 1.001) and (β, γ)=(0.481, 0.995) with T_C=0.078 from the Arrott-Noakes and KF methods (see Fig. 7(d) and (e) associated with the insets), respectively. According to the Widom scaling relation, we obtain δ=3.089 and δ=3.068, which agree with the critical isotherm measurement δ=2.997, as shown in Fig. 7(f). Meanwhile, the local exponent $n(T_C)$=0.648 is obtained from both the Arrott-Noakes and KF methods, which coincides with the MCE value. Note that the critical exponents we obtained are close to the mean field prediction ($n(T_C)$=2/3, β=0.5, γ=1.0 and δ=3.0).

These critical exponents can also be further confirmed by the scaling equation. First, we turn our attention to the Modified Arrott Plots, plotting $M^{1/\beta}$ versus $(h/M)^{1/\gamma}$ with the critical exponents obtained by KF method, as shown in Fig. 8(a) and (b). The lines are parallel and spaced linearly in temperature. Notably, the $M^{1/\beta}$ versus $(h/M)^{1/\gamma}$ line goes through the origin at T_C. In addition, in the

asymptotic critical region, the critical exponents can also be confirmed by the magnetic scaling equation:[39-41]

$$M\left(h,t\right)=t^{\beta}f_{\pm}\left(h/t^{\beta+\gamma}\right), \qquad (19)$$

where $f_{\pm}$ are regular functions denoted as f_{+} for $T>T_C$ and f_{-} for $T<T_C$. It indicates that $M|t|^{-\beta}$ versus $h|t|^{-(\beta+\gamma)}$ forms two universal curves for $T>T_C$ and $T<T_C$, respectively. Based on the scaling equation, the lg-lg scales of isothermal magnetization around the critical temperatures are plotted in Fig. 8(c) and (d) for V=1.0 and 2.0, wherein the data points fall on two independent branches. The last confirmation of validity of the obtained critical exponents would come from checking the scaling of the magnetization curves, which takes the form,[44,45]

$$\frac{h}{M^{\delta}}=H\left(\frac{t}{M^{1/\beta}}\right), \qquad (20)$$

with $H(x)$ a scaling function. Therefore, based on the above equation, if the critical exponent values are appropriate, the plot of $M/h^{1/\delta}$ versus $t/h^{1/(\beta+\gamma)}$ should correspond to a universal curve with all data points collapse. Herein, we still adopt the values obtained from KF method, the scaled data is plotted in the insets of Fig. 8(c) and (d). It presents an excellent overlap of data points, indicating that the obtained critical exponent values are good in agreement with the scaling hypothesis. On the whole, the obedience of the scaling equation over the entire range of normalized variables confirms the reliability of the obtained critical exponents.

4. Conclusions

In conclusion, the magnetocaloric effect and critical behavior of a periodic Anderson-like organic polymer are investigated by means of Green's function theory, in which the localized *f* orbitals hybridize with the conduction orbitals at even sites. We explore the field-induced ground state phase diagram with ferrimagnetic insulator, metal and ferromagnetic insulator states unveiled.

The quantum criticality is clearly demonstrated by the Grüneisen parameter which shows $|\Gamma_h| \sim T^{-1}$ power-law critical behaviour and diverges rapidly upon cooling down to zero temperature as h approaches the critical fields, providing a novel thermodynamic means for probing QPTs.

At finite temperatures, the magnetic entropy change ($-\Delta S$) presents a double peak structure for the dominant Kondo coupling case as a result from the competition of up-spin and down-spin hole excitations, implying a double magnetic cooling process via demagnetization. Meanwhile, the magnetic entropy change follows a power law dependence of magnetic field h: $-\Delta S \sim h^n$. The local exponent n tends to 1 and 2 below and above T_C, while reaches a minimum 0.648 at T_C, which is consistent with the experimental observation on perovskite manganites $Pr_{0.55}Sr_{0.45}MnO_3$ and $Nd_{0.55}Sr_{0.45}MnO_3$ corresponding to the conventional ferromagnets within the mean field theory $-\Delta S \sim h^{2/3}$. At T_C, the $-\Delta S \sim h$ curves with convex curvature superpose each other for small V values, which are separated by the large V case, distinguishing the RKKY interaction and Kondo coupling explicitly. Furthermore, the critical scaling law $n(T_C)=1+(\beta-1)/(\beta+\gamma)=1+1/\delta(1-1/\beta)$ is related to the critical exponents (β, γ, and δ) extracted from the Arrott-Noakes equation of state and Kouvel-Fisher method, which fulfill the Widom scaling relation $\delta=1+\gamma\beta^{-1}$, indicating self-consistency and reliability of the obtained results. In addition, based on the scaling hypothesis through checking the scaling analysis of magnetization, the lg-lg scales of $M|t|^{-\beta}$ versus $h|t|^{-(\beta+\gamma)}$ collapse onto two independent universal branches for $T>T_C$ and $T<T_C$, respectively, while the plot of $M/h^{1/\delta}$ versus $t/h^{1/(\beta+\gamma)}$ forms one universal curve with all data points collapse, which further confirm the reliability of the obtained critical exponents over the entire range of normalized variables.

Acknowledgement

This work was supported by the National Natural Science Foundation of China under Grant No. 11204157, 11174179 and 11247020.

References

1 A. M. Tishin and Y. I. Spichkin, *The magnetocaloric effect and its applications* (Institute of Physics Publishing, Bristol and Philadelphia, 2003).

2 N. A. de Oliveira and P. J. von Ranke, *Phys. Rep*., 2010, **489**, 89.

3 E. Brück, *J. Phys. D: Appl. Phys*., 2005, **38**, R381.

4 L. Mañosa, A. Planes and M. Acet, *J. Mater. Chem. A*, 2013, **1**, 4925.

5 Y. Y. Gong, D. H. Wang, Q. Q. Cao, E. K. Liu, J. Liu and Y. W. Du, *Adv. Mater.*, 2015, **27**, 801.

6 S. Nayak, M. Evangelisti, A. K. Powell and J. Reedijk, *Chem. Eur. J*., 2010, **16**, 12865.

7 J. L. Liu, W. Q. Lin, Y. C. Chen, S. Gómez-Coca, D. Aravena, E. Ruiz, J. D. Leng and M. L. Tong, *Chem. Eur. J*., 2013, **19**, 17567.

8 M. Evangelisti, O. Roubeau, E. Palacios, A. Camón, T. N. Hooper, E. K. Brechin and J. J. Alonso, *Angew. Chem. Int. Ed*., 2011, **50**, 6606.

9 Y.C. Chen, L. Qin, Z. S. Meng, D. F. Yang, C. Wu, Z. D. Fu, Y. Z. Zheng, J. L. Liu, R. Tarasenko, M. Orendáč, J. Prokleška, V. Sechovský and M. L. Tong, *J. Mater. Chem. A*, 2014, **2**, 9851.

10 H. C. Hu, C. S. Cao, Y. Yang, P. Cheng and B. Zhao, *J. Mater. Chem. C*, 2015, **3**, 3494.

11 H. C. Hu, X. M. Kang, C. S. Cao, P. Cheng and B. Zhao, *Chem. Commun*., 2015, **51**, 10850.

12 B. Wolfa, Y. Tsuia, D. Jaiswal-Nagara, U. Tutscha, A. Honeckerb, K. Remović-Langera, G. Hofmanna, A. Prokofievc, W.Assmusa, G. Donathd and M. Langa, *Proc. Natl. Acad. Sci.*

USA, 2011, **108**, 6862.

13 M. Garst and A. Rosch, *Phys. Rev. B*, 2005, **72**, 205129.

14 A. W. Rost, R. S. Perry, J. F. Mercure, A. P. Mackenzie and S. A. Grigera, *Science*, 2009, **325**, 1360.

15 H. Ryll, K. Kiefer, Ch. Rüegg, S. Ward, K.W. Krämer, D. Biner, P. Bouillot, E. Coira, T. Giamarchi, and C. Kollath, *Phys. Rev. B*, 2014, **89**, 144416.

16 J. S. Miller, *Adv. Mater*., 2002, **14**, 1105.

17 W. Fujita, K. Kikuchi and K. Awaga, *Angew. Chem. Int. Ed*., 2008, **47**, 9480.

18 E. Lieb, T. Schultz and D. Mattis, *Annals of Phys*., 1961, **16**, 407.

19 V. Franco, A. Conde, *Int. J. Refrig*., 2010, **33**, 465.

20 Y. T. Su, Y. Sui, J. G. Cheng, J. S. Zhou, X. J. Wang, Y. Wang and J. B. Goodenough, *Phys. Rev. B*, 2013, **87**, 195102.

21 A. Biswas, S. Chandra, T. Samanta, B. Ghosh, S. Datta, M. H. Phan, A. K. Raychaudhuri, I. Das and H. Srikanth, *Phys. Rev. B*, 2013, **87**, 134420.

22 J. Y. Fan, L. Pi, L. Zhang, W. Tong, L. S. Ling, B. Hong, Y. G. Shi, W. C. Zhang, D. Lu and Y. H. Zhang, *Appl. Phys. Lett*., 2011, 98, 072508.

23 L. S. Xu, J. Y. Fan, Y. G. Shi, Y. Zhu, K. Bärner, C. P. Yang and D. N. Shi, Europhys. Lett., 2015, **112**, 17005.

24 S. N. Kaul, *J. Magn. Magn. Mater*., 1985, **53**, 5.

25 A. A. Ovchinnikov, *Theoret. Chim. Acta*, 1978, **47**, 297.

26 M. A. Hajj and J. P. Malrieu, *J. Chem. Phys*., 2007, **127**, 144902.

27 L. Zhao, K. L. Yao and Y. F. Duan, *Phys. Chem. Chem. Phys*., 2000, **2**, 4001.

28 W. Z. Wang, *Phys. Rev. B*, 2006, **73**, 035118.

29 L. J. Ding, K. L. Yao and H. H. Fu, *Phys. Chem. Chem. Phys*., 2011, **13**, 328.

30 M. F. Crommie, *Science*, 2005, **309**, 1501.

31 C. A. Hooley and A. P. Mackenzie, *Science*, 2007, **137**, 1332.

32 H. Tsunetsugu, M. Sigrist and K. Ueda, Rev. Mod. Phys., 1997, **69**, 809.

33 P. Fröbrich and P. J. Kuntz, Phys. Rep., 2006, **432**, 223.

34 N. A. Zimbovskaya, *Phys. Rev. B*, 2008, **78**, 035331.

35 V. Franco, J. S. Blázquez and A. Conde, *Appl. Phys. Lett*., 2006, **89**, 222512.

36 H. Oesterreicher and F. T. Parker, *J. Appl. Phys*., 1984, **55,** 4334.

37 L. A. Burrola-Gándara, C. R. Santillan-Rodriguez, F. J. Rivera-Gomez, R. J. Saenz-Hernandez, M. E. Botello-Zubiate and J. A. Matutes-Aquino, *J. Appl. Phys*., 2015, **117**, 17D144.

38 A. Arrott and J. E. Noakes, *Phys. Rev. Lett.*, 1967, **19**, 786.

39 L. Zhang, J. Fang, J. Y. Fan, M. Ge, L. S. Ling, C. J. Zhang, L. Pi, S. Tan, Y. H. Zhang, *J. Alloy Comp*., 588 (2014) 294–299

40 L. Zhang, D. Menzel, C. M. Jin, H. F.Du, M. Ge, C. J. Zhang, L. Pi, M. L. Tian and Y. H. Zhang, *Phys. Rev. B*, 2015, **91**, 024403.

41 E. Svanidze, L. Liu, B. Frandsen, B. D. White, T. Besara, T. Goko, T. Medina, T. J. S. Munsie, G. M. Luke, D. Zheng, C. Q. Jin, T. Siegrist, M. B. Maple, Y. J. Uemura and E. Morosan, *Phys. Rev. X*, 2015, **5**, 011026.

42 J. S. Kouvkl and M. E. Fisher, *Phys. Rev*., 1964, **136,** A1626.

43 B. Widom, *J. Chem. Phys*., 1965, **43**, 3898.

44 M. H. Phan, V. Franco, A. Chaturvedi, S. Stefanoski, G. S. Nolas and H. Srikanth, *Phys. Rev. B*,

2011, **84**, 054436.

45 V. Franco, R. Caballero-Flores, A. Conde, K. E. Knipling and M. A. Willard, *J. Appl. Phys*., 2011, **109**, 07A905.

Figures and Figure captions:

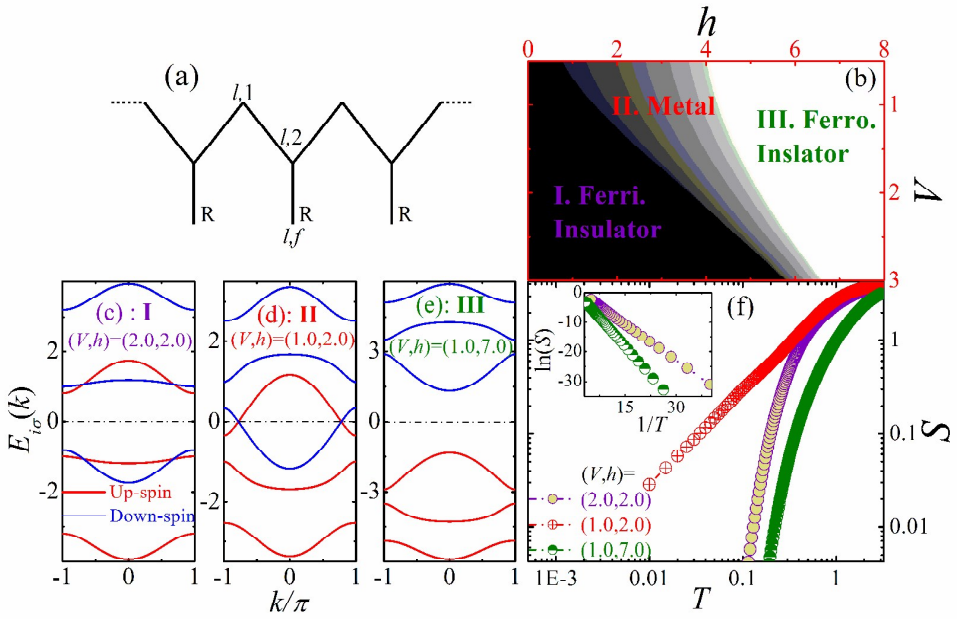

Fig. 1 (Color online) (a) Schematic illustration of a quasi-one-dimensional periodic Anderson-like organic polymer chain; (b) the *h*-*V* phase diagram with (I) ferrimanetic insulator, (II) metal and (III) ferromagnetic insulator phases, which are demonstrated by the energy bands in (c), (d) and (e), respectively; (f) the temperature dependence of entropy *S*, ln(*S*)-1/*T* curve is plotted in the inset.

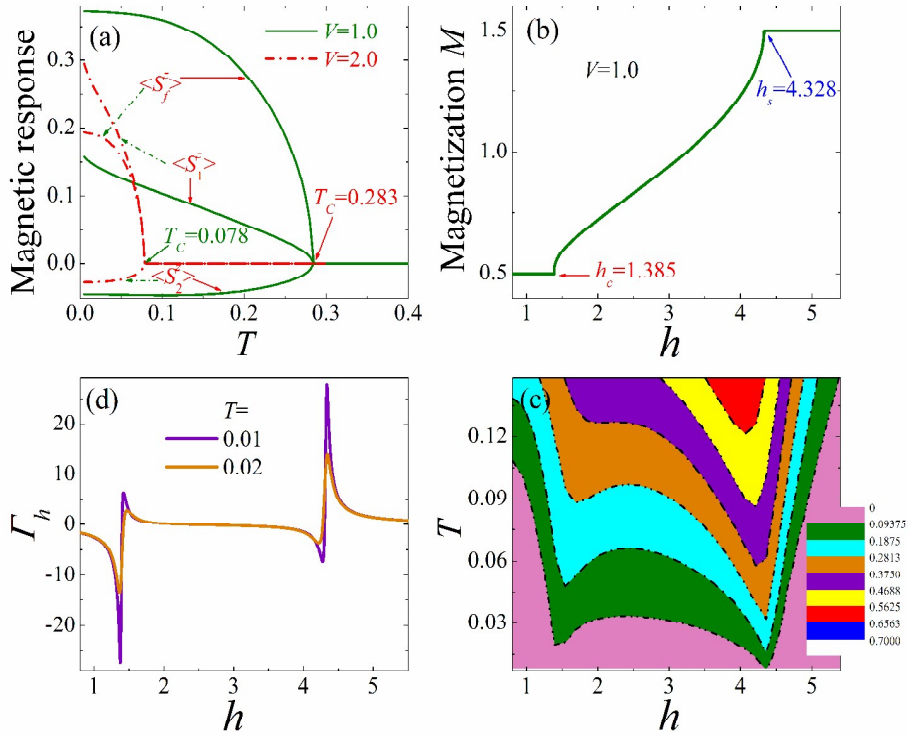

Fig. 2 (Color online) (a) The temperature dependence of sublattice magnetization; (b) the field dependence of magnetization for V=1.0; (c) the isoentropes for V=1.0; (d) the field dependence of Grüneisen parameter Γ_h at different temperatures.

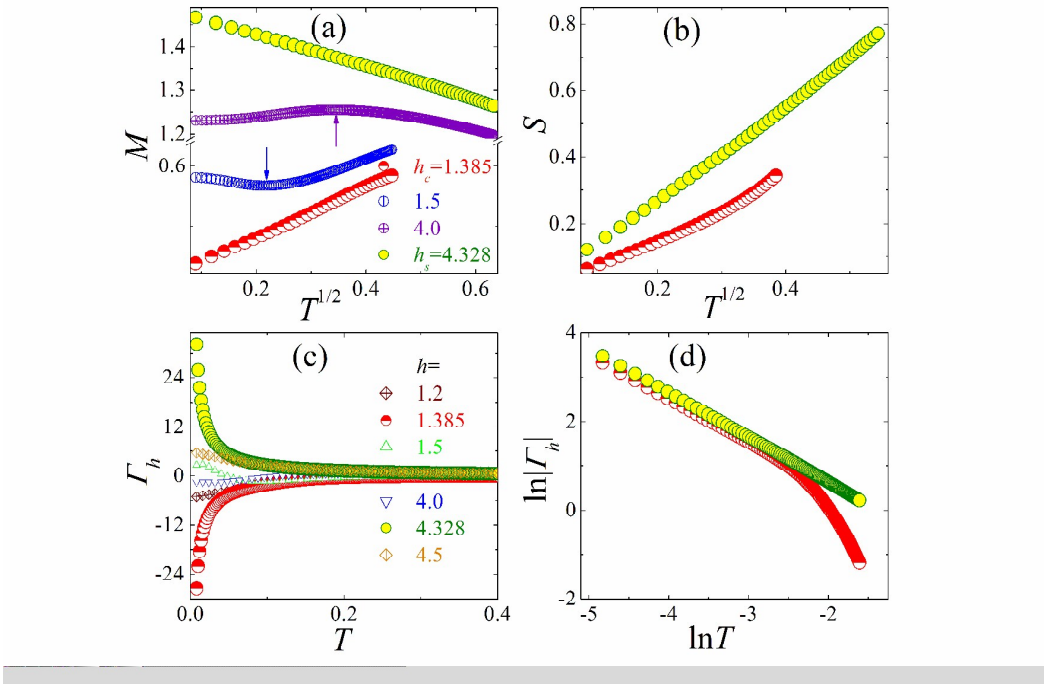

Fig. 3(Color online) (a) the magnetization M and (b) entropy S as a function of $T^{1/2}$ under different fields; (c) the temperature dependence of Grüneisen parameter Γ_h under different fields; (d) $\ln|\Gamma_h|$ versus ln$T$ at the critical fields.

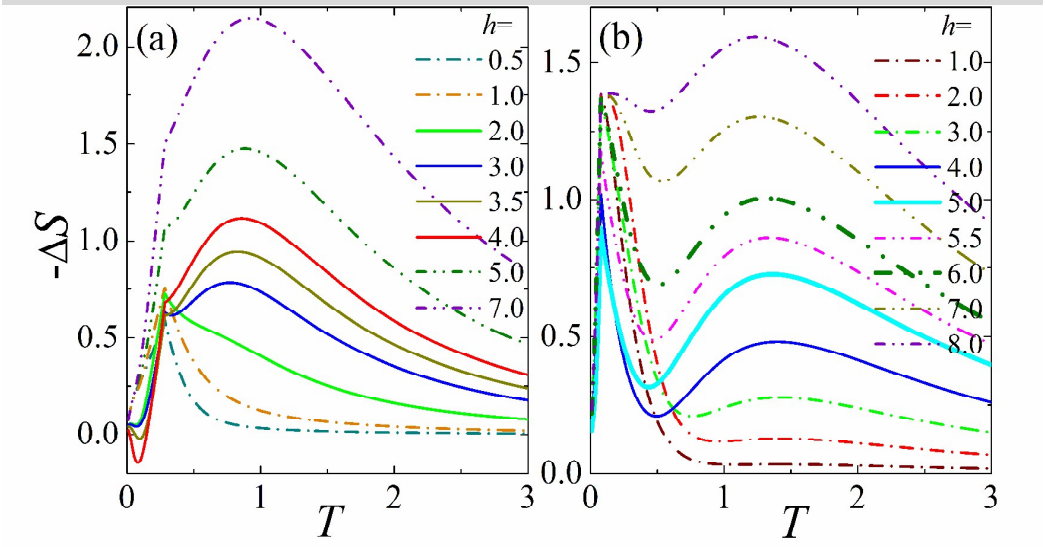

Fig. 4 (Color online) The temperature dependence of magnetic entropy change (-Δ*S*) for (a) *V*=1.0 and (b) *V*=2.0.

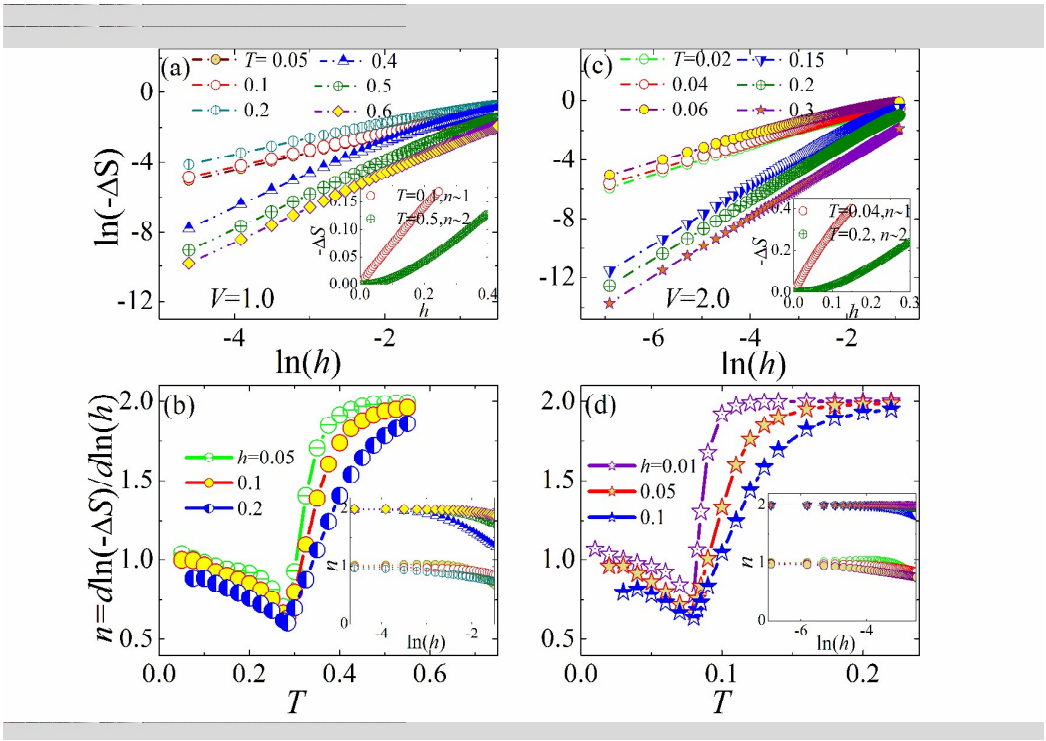

Fig.5 (Color online) ln(-Δ*S*) versus ln(h) at different temperatures for (a) *V*=1.0 and (b) *V*=2.0; the insets are the field dependence of –Δ*S* for the temperature below and above T_C; The corresponding local exponent $n=d\ln(-\Delta S)/d\ln(h)$ as a function of temperature in (c) and (d), respectively; the insets show the local exponent *n* against ln(*h*) for the temperature below and above T_C, respectively.

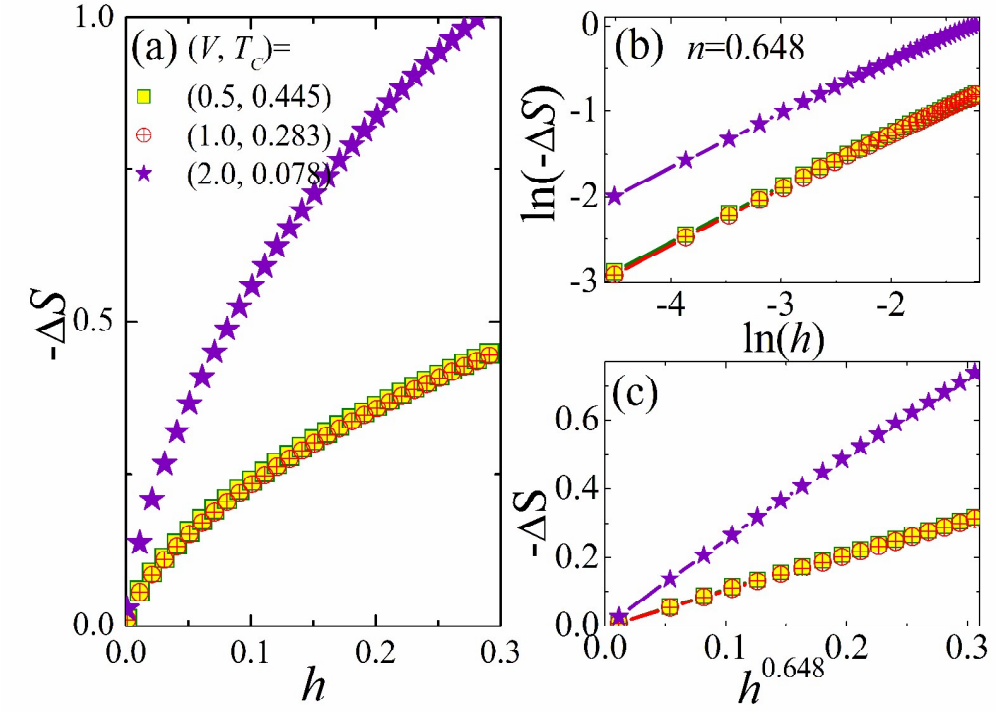

Fig. 6 (Color online) (a) The field dependence of $-\Delta S$ for $T=T_C$ with different V values; (b) double-logarithm of $-\Delta S$-h curves for $T=T_C$; (c) the linear behaviour of $-\Delta S$-$h^{0.648}$.

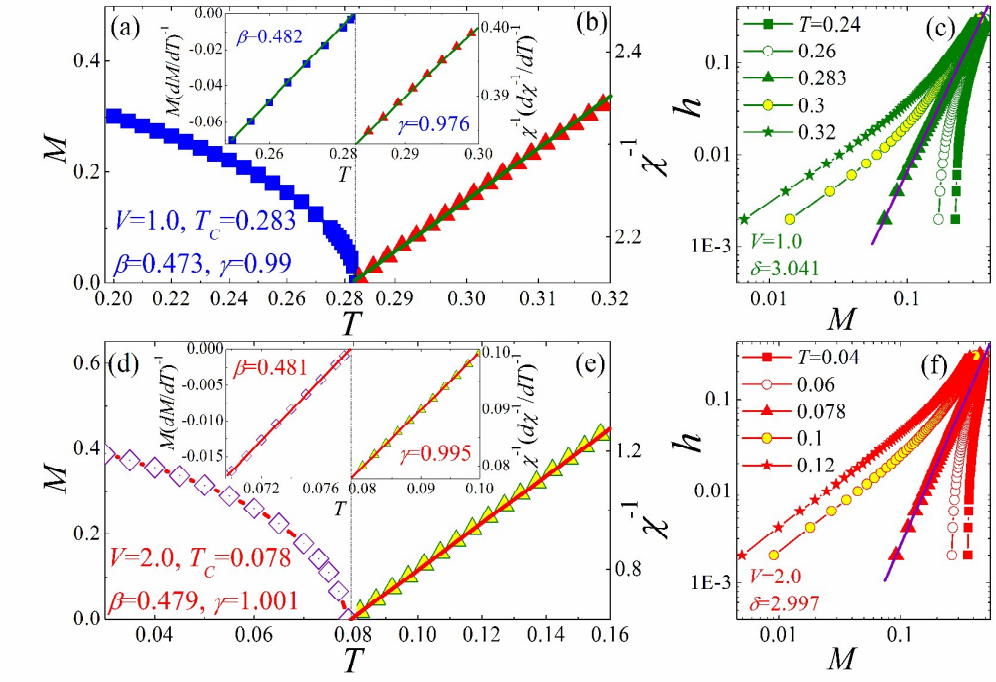

Fig. 7 (Color online) For V=1.0, the temperature dependence of (a) magnetization M and (b) inverse initial susceptibility χ^{-1}; For V=2.0 the temperature dependence of (d) magnetization M and (e) inverse initial susceptibility χ^{-1}; the insets are the KF plots; the lg-lg scale of h-M curves for (c) V=1.0 and (f) V=2.0.

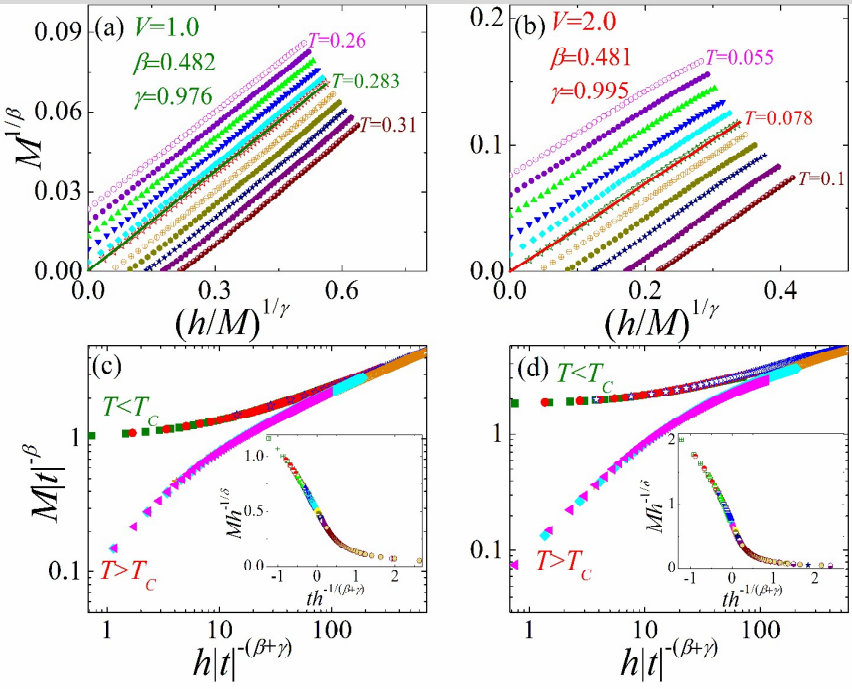

Fig. 8 (Color online) The isotherms $M^{1/\beta}$ vs $(h/M)^{1/\gamma}$ for (a) V=1.0 and (b) V=2.0; scaling plots around T_C for (c) V=1.0 and (d) V=2.0; the insets are the normalized isotherms below and above T_C using the values of β and γ determined by the KF method.